Review and Assessment of the Steep Lifting Entry Closed-Form Trajectory Solution

Zachary R. Putnam*
University of Illinois at Urbana-Champaign, Urbana, Illinois, 61801
and
Robert D. Braun†
Georgia Institute of Technology, Atlanta, Georgia, 30332

The complete, historical closed-form steep lifting entry trajectory solution is documented and developed from first principles. The efficacy and accuracy of the solution is assessed for application to aeroassist missions of interest, including aerocapture and entry. Specifically, analytical assessment of the primary assumptions in the solution shows the solution is applicable across a wide range of initial states for vehicles with nonzero lift-to-drag ratios. Solution accuracy is assessed relative to the planar equations of motion; accuracy improves for steeper trajectories and larger lift-to-drag ratios. The steep lifting entry estimate of peak acceleration is shown to be accurate to within 10% for initial flight-path angles steeper than approximately -10 deg across a variety of vehicles, missions, and planetary destinations. Overall, the steep lifting entry solution provides a simple, rapid first-order trajectory solution capability for lifting aeroassist vehicles with relatively steep initial flight-path angles.

Nomenclature

a	=	acceleration magnitude, surface g
c	=	constant
C_D	=	hypersonic drag coefficient
C_L	=	hypersonic lift coefficient
D	=	$\bar{q}S_{ref}C_D$, drag magnitude, N
g	=	acceleration due to gravity, m/s^2
H	=	atmospheric scale height, m
h	=	altitude, m
h_{ref}	=	reference altitude, m
L	=	$\bar{q}S_{ref}C_L$, lift magnitude, N
L/D	=	lift-to-drag ratio
m	=	mass, kg
$\bar{q}$	=	$\rho V^2/2$, dynamic pressure, N/m^2
R	=	planetary radius, m
s	=	range over planetary surface, km
S_{ref}	=	aerodynamic reference area, m^2
t	=	time, s
V	=	velocity magnitude, m/s
V_C	=	$\sqrt{gR}$, circular speed, m/s
β	=	$m/(C_D S_{ref})$, ballistic coefficient, kg/m^2
γ	=	flight-path angle, positive above local horizontal, rad
ρ	=	atmospheric density, kg/m^3

*Assistant Professor, Department of Aerospace Engineering, 104 S. Wright St., Senior Member AIAA.
†Professor, School of Aerospace Engineering, 270 Ferst Dr., Fellow AIAA.

ρ_{ref} = density at reference altitude, kg/m^3
θ = range angle, rad

Subscripts
0 = initial value
f = final value
max = maximum value

I. Introduction

Analytical approximate solutions to the nonlinear equations of motion governing aeroassist trajectories were developed in the middle of the twentieth century to enable vehicle and mission designers to evaluate vehicle performance with minimal computer usage. Modern computing systems provide a relatively rapid, low-cost, and high-fidelity assessment capability for aeroassist trajectories through numerical integration of the equations of motion.[1] However, analytical approximate solutions are still desirable for applications where simplicity and execution speed are paramount, such as real-time guidance, navigation, and control systems; optimization; and conceptual design. Furthermore, closed-form analytical solutions provide information about entire classes of aeroassist trajectories: the solutions may be manipulated to determine driving parameters and sensitivities without requiring specific vehicle, mission, or environment data.

Multiple approximate solutions for planar, lifting aeroassist trajectories have been developed. The equilibrium glide solution developed by Sänger and Bredt in the 1940s is perhaps the best-known of these approximate solutions.[2] The equilibrium glide solution works well for shallow trajectories with relatively large lift-to-drag ratios. Two generally-applicable solutions, valid for any lift-to-drag ratio, were developed in the 1960s: Loh's "second-order" implicit solution[3] and the solution of Citron and Meir.[4] As a consequence of their generality, these solutions are mathematically more complicated than others and do not include expressions for all quantities of interest, such as range. In contrast to these solutions, the steep lifting entry solution approximates steep trajectories with a solution complexity similar to that of equilibrium glide.

The steep lifting entry solution was primarily developed in the 1950s and 60s by Eggers, Allen, and Niece of the National Advisory Committee for Aeronautics Ames Aeronautical Laboratory;[5] Lees, Hartwig, and Cohen of Space Technologies, Inc. for the U.S. Air Force;[6] and Wang and Ting of the Polytechnic Institute of Brooklyn, also supported by the U.S. Air Force.[7] Additional contributions were made by Miele and Vinh et al., who developed expressions for flight range, and Vinh et al., who applied the solution to aerocapture trajectories in 2000.[8] Portions of the steep lifting entry solution are documented in flight dynamics texts,[9–11] but no complete treatment of the solution is available in the literature. Furthermore, many of these primary sources are out of print and difficult to access.

This paper develops the complete, historical steep lifting entry solution from first principles to preserve it for future researchers. The accuracy and efficacy of the solution and its components are evaluated to inform future applications.

II. Derivation of the Steep Lifting Entry Solution

The complete, historical derivation of the steep lifting entry trajectory solution is presented in consistent nomenclature. The solution is compiled from several primary sources and includes expressions for velocity, sensed acceleration, density (or altitude), and range as functions of flight-path angle.

A. Equations of Motion

The planar equations of motion for a planetary entry vehicle may be written as:[10]

$$\frac{dV}{dt} = -\frac{\rho V^2}{2\beta} - g\sin\gamma \tag{1a}$$

$$\frac{d\gamma}{dt} = \frac{V\cos\gamma}{R+h} + \frac{\rho V}{2\beta}\left(\frac{L}{D}\right) - \frac{g\cos\gamma}{V} \tag{1b}$$

$$\frac{dh}{dt} = V\sin\gamma \tag{1c}$$

$$\frac{d\theta}{dt} = \frac{V\cos\gamma}{R+h} \tag{1d}$$

where the flight-path angle γ is defined to be positive above the local horizontal. While all aeroassist trajectories exhibit some out-of-plane motion, the bulk of the motion occurs in a single plane and many trajectory parameters of interest may be determined through analysis of the planar motion. Eq. (1) is a set of coupled, first-order, ordinary differential equations. These equations are highly nonlinear due to the presence of the planetary atmosphere and trigonometric functions and defy analytical solution unless simplifying assumptions are applied.

The primary assumptions in the steep lifting entry solution, relative to Eq. (1), are neglecting the gravity and curvature terms relative to the aerodynamic force terms in the equations of motion. These assumptions are appropriate for steep trajectories where aerodynamic forces are large, a key family of trajectories that are not well-approximated by the equilibrium glide solution. The definition of a lifting trajectory is straightforward: a trajectory with nonzero L/D. The definition of a "steep" trajectory is less straightforward. Analyses presented in subsequent sections show that, for the steep lifting entry solution, trajectories with initial flight-path angles steeper than approximately -10 deg are sufficiently steep.

B. Eggers, Allen, and Neice's Skip-Entry Solution

In the mid-1950s, Eggers, Allen, and Neice developed closed-form analytical solutions for lifting hypersonic trajectories. Their original research memorandum was considered confidential;[12] subsequent versions were not.[5,13] Their primary interest was modeling the atmospheric flight portion of a multiple-skip entry trajectory that could be used to extend the range of a hypersonic vehicle. The primary assumptions used by Eggers et al. were neglecting gravity in both the lift and drag equations (Eq. (1b) and Eq. (1a), respectively) and the planetary curvature term in the lift equation (Eq. (1b)). While large L/D and a steep initial flight-path angle were not explicit assumptions, it is under these conditions that the assumptions of Eggers et al. are valid.

Starting with Eq. (1b) and neglecting the gravity term relative to the aerodynamic term ($g/V\cos\gamma \ll (L/D)\rho V/(2\beta)$) and assuming a flat planet ($R \to \infty$) results in:

$$\frac{d\gamma}{dt} = \frac{\rho V}{2\beta}\left(\frac{L}{D}\right) \tag{2}$$

The time derivative of the flight-path angle may expanded to:

$$\frac{d\gamma}{dt} = \frac{d\gamma}{dV}\frac{dV}{dt} \tag{3}$$

If one neglects the drag term relative to the aerodynamic term in Eq. (1a), one can write:

$$\frac{dV}{dt} = -\frac{\rho V^2}{2\beta} \tag{4}$$

Combining Eq. (2), Eq. (3), and Eq. (4) and separating variables results in:

$$d\gamma = -\left(\frac{L}{D}\right)\left(\frac{1}{V}\right)dV \tag{5}$$

Integrating from an initial state (γ_0, V_0) to some other state (γ, V) results in a closed-form expression for flight-path angle in terms of velocity:

$$\gamma = \gamma_0 - \left(\frac{L}{D}\right) \ln\left(\frac{V}{V_0}\right) \tag{6}$$

Or, for velocity in terms of flight-path angle:

$$V = V_0 \exp\left(\frac{\gamma_0 - \gamma}{L/D}\right) \tag{7}$$

Eq. (6) and Eq. (7) make no assumptions about the variation of atmospheric density over the trajectory; they are valid for any planetary atmosphere or atmosphere model. If an exponential atmosphere is assumed, such that $\rho = \rho_{ref} \exp\left[(h_{ref} - h)/H\right]$, then:

$$\frac{dh}{dt} = -\frac{H}{\rho}\frac{d\rho}{dt} \tag{8}$$

Substituting this expression into Eq. (1c) results in:

$$-\frac{H}{\rho}\frac{d\rho}{dt} = V \sin\gamma \tag{9}$$

Solving Eq. (2) for velocity yields:

$$V = \frac{d\gamma}{dt}\frac{2\beta}{\rho(L/D)} \tag{10}$$

Substituting Eq. (10) for V in Eq. (9) and simplifying results in:

$$d\rho = -\frac{2\beta \sin\gamma}{H(L/D)} d\gamma \tag{11}$$

Integrating from the initial state (γ_0, ρ_0) to some other state (γ, ρ) results in:

$$\rho = \rho_0 + \frac{2\beta}{H(L/D)} \left(\cos\gamma - \cos\gamma_0\right) \tag{12}$$

Eq. (12) may also be written in terms of altitude:

$$h = h_{ref} - H \ln\left[\exp\left(\frac{h_{ref} - h_0}{H}\right) + \frac{2\beta}{H\rho_{ref}(L/D)} \left(\cos\gamma - \cos\gamma_0\right)\right] \tag{13}$$

From Eq. (12) and Eq. (13) Eggers et al. realized that the flight-path angle at atmospheric entry and exit must be equal and opposite on a skip trajectory because the vehicle returns to the same altitude and the cosine of the flight-path angle is symmetric about zero.

C. Expressions for Acceleration

Lees, Hartwig, and Cohen extended the theory of Eggers et al. in 1958 by developing an expression for the sensed acceleration in terms of the flight-path angle (a more concise version was published in 1959).[6,14] Lees et al. point out that they make subtly different, though mathematically equivalent, assumptions to simplify the equations of motion relative to Eggers et al. Specifically, Lees et al. assume that the difference between the centrifugal and gravitational terms is negligible relative to the aerodynamic force in Eq. (1b). This assumption is particularly good for trajectories with velocities near the circular speed; it contrasts with the separate assumptions of a flat planet and negligible gravity made by Eggers et al.

The sensed deceleration, expressed in surface g, is given by:

$$a = \sqrt{\left(\frac{L}{mg}\right)^2 + \left(\frac{D}{mg}\right)^2} = \frac{\rho V^2}{2g\beta}\sqrt{1 + (L/D)^2} \tag{14}$$

Plugging in expressions for density (Eq. (12)) and velocity (Eq. (7)) into Eq. (14) yields an expression for sensed acceleration as a function of flight-path angle:

$$a = \left[\frac{\rho_0}{2g\beta} + \frac{\cos\gamma - \cos\gamma_0}{gH(L/D)}\right] V_0^2 \sqrt{1 + (L/D)^2} \exp\left[\frac{2\left(\gamma_0 - \gamma\right)}{L/D}\right] \tag{15}$$

From Eq. (14), it is apparent that peak acceleration occurs when the dynamic pressure is a maximum, or when:

$$\frac{d\bar{q}}{dt} = -\frac{\rho V^3}{\rho_{ref} H}\left(\sin\gamma + \frac{H}{\beta}\rho\right) = 0 \tag{16}$$

The flight-path angle at peak acceleration is then given by (again, neglecting gravity relative to drag in Eq. (1a)):

$$\sin\gamma_{a_{max}} = -\frac{H}{\beta}\rho_{a_{max}} = -\frac{H}{\beta}\left[\rho_0 + \frac{2\beta}{H(L/D)}\left(\cos\gamma_{a_{max}} - \cos\gamma_0\right)\right] \tag{17}$$

This expression is transcendental in $\gamma_{a_{max}}$. If one assumes $\gamma_{a_{max}}$ is small, then $\sin\gamma \approx \gamma$ and $\cos\gamma \approx 1 - \gamma^2/2$, resulting in an expression that is quadratic in $\gamma_{a_{max}}$:

$$\gamma_{a_{max}} \approx -\frac{H}{\beta}\left[\rho_0 + \frac{\beta}{H(L/D)}\left(\gamma_0^2 - \gamma_{a_{max}}^2\right)\right] \tag{18}$$

The flight-path angle at peak acceleration may then be approximated as:

$$\gamma_{a_{max}} = \frac{L/D}{2} - \frac{1}{2}\sqrt{(L/D)^2 + 4\left(\gamma_0^2 + \frac{H\rho_0(L/D)}{\beta}\right)} \tag{19}$$

Lees et al. utilized their theory to assess the capability of discrete-event lift-modulation trajectory control to limit peak acceleration during entry.

The work of Lees et al. was in turn extended to greater entry velocities by Wang and Ting in 1960.[7,15] Wang and Ting demonstrated that the gravity term in the lift equation may be retained (Eq. (1b)), resulting in:

$$\gamma = -\sqrt{\gamma_0^2 + 2H\left(\frac{g}{V_0^2} - \frac{1}{R}\right)\ln\left(\frac{\rho}{\rho_0}\right) - \frac{H(L/D)}{\beta}\left(\rho - \rho_0\right)} \tag{20}$$

To retain the gravity term, Wang and Ting assume the difference of the centrifugal and gravity terms in Eq. (1b), and therefore the velocity, is constant from the initial state at the top of the atmosphere to peak acceleration. The density and flight-path angle at peak acceleration may then be computed by assuming the flight-path angle at peak deceleration is small in Eq. (17), such that:

$$\gamma_{a_{max}} = -(H/\beta)\rho_{a_{max}} \tag{21}$$

Eq. (21) may be substituted into Eq. (20) to create implicit expressions for $\rho_{a_{max}}$ and $\gamma_{a_{max}}$ that must be solved iteratively.

Wang and Ting also developed an expression for the velocity at peak acceleration. Dividing Eq. (9) by Eq. (4) and assuming γ is small yields:

$$dV/V = H/(2\beta\gamma)d\rho \tag{22}$$

Substituting Eq. (20) into Eq. (22) and replacing the $\ln(\rho/\rho_0)$ factor in Eq. (20) with a Mercator series expansion makes Eq. (22) analytically integrable, resulting in:

$$V_{a_{max}} = V_0 \exp\left[-\frac{H}{2\beta\sqrt{c_3}}\ln\frac{\sqrt{c_3\left(c_1 + c_2\rho_{a_{max}} + c_3\rho_{a_{max}}^2\right)} + c_3\rho_{a_{max}} + c_2/2}{\sqrt{c_3\left(c_1 + c_2\rho_0 + c_3\rho_0^2\right)} + c_3\rho_0 + c_2/2}\right] \tag{23}$$

where:

$$c_1 = \gamma_0^2 + H\rho_0(L/D)/\beta - 3H\left(g/V_0^2 - 1/R\right) \tag{24a}$$

$$c_2 = 4H\left(g/V_0^2 - 1/R\right)/\rho_0 - H(L/D)/\beta \tag{24b}$$

$$c_3 = -H\left(g/V_0^2 - 1/R\right)/\rho_0^2 \tag{24c}$$

While more complicated, the expressions developed by Wang and Ting offer accuracy advantages over those of Eggers et al. and Lees et al. for some trajectories.

D. Expression for Range

In their analysis of long-range skipping trajectories in Ref. 5, Eggers et al. neglected the range traveled during the atmospheric flight segments. Inclusion of the atmospheric flight range improves total range estimates for multi-skip entries and provides range estimates for direct entries. An expression for range during atmospheric flight may be derived starting from Eq. (1d). Assuming $R \gg h$ gives:

$$\frac{d\theta}{dt} = \frac{V\cos\gamma}{R} \tag{25}$$

Or:

$$R\frac{d\theta}{dt} = \frac{ds}{dt} = V\cos\gamma \tag{26}$$

Substituting Eq. (10) for V and simplifying gives:

$$ds = \frac{2\beta}{(L/D)}\frac{\cos\gamma}{\rho}d\gamma \tag{27}$$

Substituting in Eq. (12) for ρ yields:

$$ds = \frac{2\beta}{(L/D)}\frac{\cos\gamma}{\rho_0 + \dfrac{2\beta}{H(L/D)}\left(\cos\gamma - \cos\gamma_0\right)}d\gamma \tag{28}$$

Integrating from the initial state $(s_0 = 0, \gamma_0)$ to the some other state (s, γ) results in:

$$s = H\left(\gamma - \gamma_0\right) + \frac{Hc_4}{\sqrt{1-c_4^2}}\ln\left\{\frac{(1-c_4)\tan\left(\frac{\gamma}{2}\right)\tan\left(\frac{\gamma_0}{2}\right) - \sqrt{1-c_4^2}\left[\tan\left(\frac{\gamma}{2}\right) - \tan\left(\frac{\gamma_0}{2}\right)\right] - c_4 - 1}{(1-c_4)\tan\left(\frac{\gamma}{2}\right)\tan\left(\frac{\gamma_0}{2}\right) + \sqrt{1-c_4^2}\left[\tan\left(\frac{\gamma}{2}\right) - \tan\left(\frac{\gamma_0}{2}\right)\right] - c_4 - 1}\right\} \tag{29}$$

where:

$$c_4 = \frac{H\rho_0}{2\beta}\left(L/D\right) - \cos\gamma_0 \tag{30}$$

This result was first obtained by Miele in 1962.[9] Vinh et al. published a similar result in 1980.[10] Eq. (29) may be used for all types of aeroassist trajectories for which the steep lifting entry assumptions are appropriate.

E. Summary

Contributions to the steep lifting entry solution and their associated assumptions are summarized in Table 1. While all of the contributions share the same core assumptions, some variance is present for specific relationships. The collected contributions of these authors describe a consistent and complete analytical approximate solution to the equations of motion for the hypersonic portions of lifting aeroassist trajectories.

III. Applicability of Solution

A. Trajectory Parameters

The steep lifting entry solution may be used for direct, loft, and skip entries, as well as aerocapture trajectories. For direct entries, the solution is valid for monotonically increasing flight-path angles less than zero. For trajectories with positive altitude rate, especially aerocapture, the steep-lifting entry solution may be applied in two segments: from the top of the atmosphere to minimum altitude (where the flight-path angle is zero) then from minimum altitude to atmospheric exit. This ensures that the flight-path angle is either monotonically decreasing or increasing for each trajectory segment.

The steep lifting entry solution is valid for $L/D \neq 0$. For lift-to-drag ratios greater than zero, the flight-path angle becomes more shallow during entry, increasing towards zero. For lift-to-drag ratios less than zero, the flight-path angle decreases during entry, becoming more steep. Eq. (6) shows that a lift-to-drag ratio of zero results in a constant flight-path angle. Since the steep-lifting solution utilizes flight-path angle for its domain, a constant flight-path angle renders the solution inert. A constant flight-path angle is a good

Table 1. Steep Lifting Entry Solutions and Assumptions

Solutions	Author(s)	Eggers, Allen, and Niece		Lees, Hartwig, and Cohen			Wang and Ting		Miele
	Relationship	$\rho(\gamma)$	$V(\gamma)$	$a(\gamma)$	a_{max}	γ at a_{max}	$\gamma(\rho)$	V at a_{max}	$s(\gamma)$
Assumptions	Planar motion	•	•	•	•	•	•	•	•
	Constant g	•	•	•	•	•	•	•	•
	Constant L/D	•	•	•	•	•	•	•	•
	Constant β	•	•	•	•	•	•	•	•
	Exponential atm.			•	•	•	•	•	•
	Flat planet	•	•						
	Negelct gravity	•	•						
	Neglect difference of centrifugal and gravity forces			•	•	•	•	•	•
	$R+h \approx R$			•	•	•	•	•	•
	γ small				•	•	•	•	
	Difference of centrifugal and gravity forces constant						•	•	

first-order approximation of a nonlifting entry trajectory; this dynamic condition is a primary assumption in the Allen-Eggers ballistic entry solution.[16]

The steep lifting entry solution is compatible with a wide range of vehicle ballistic coefficients. While ballistic coefficient only has a second-order effect on the accuracy of the solution, one must take care to ensure the ballistic coefficient is small enough such that assumption that aerodynamic forces dominate gravitational forces is valid (see Eq. (4)). However, from a practical perspective, vehicles with large ballistic coefficients (e.g. strategic reentry systems) are typically associated with trajectories with steep initial flight-path angles, alleviating this concern.

B. Assumptions

The two central assumptions in the steep lifting entry trajectory approximation are that the difference of the range-angle and gravity terms is much smaller than the lift term in the flight-path angle equation (Eq. (1b)) and that the drag term is much greater than the gravity term in the velocity equation (Eq. (1a)). These assumptions may be used to bound the vehicle-trajectory design space for which the steep lifting solution solution is applicable.

The assumption neglecting the difference of the range-angle and gravity terms in Eq. (1b), as first made by Lees et al. may be stated as:

$$\frac{\rho V^2}{2\beta}(L/D) \gg \left| \frac{V^2 \cos\gamma}{R+h} - g\cos\gamma \right| \tag{31}$$

Assuming that $R \gg h$ and recognizing that $\cos\gamma$ is always positive, one can write:

$$\frac{\rho V^2}{2\beta}(L/D) \gg \left| \frac{V^2}{R} - g \right| \cos\gamma \tag{32}$$

This condition must be satisfied throughout a particular trajectory for the approximate solution to be valid. This expression may be integrated over a trajectory to examine how well it is satisfied over that trajectory. To facilitate integration, Eq. (32) may be re-written as:

$$\frac{\rho V^2}{2\beta}(L/D) \gg \begin{cases} \left(\frac{V^2}{R} - g\right)\cos\gamma & \text{if } V \geq V_C \\ \left(g - \frac{V^2}{R}\right)\cos\gamma & \text{if } V < V_C \end{cases} \tag{33}$$

This expression may be integrated in a piecewise fashion: from the initial condition to V_C and from V_C to the final condition. The integral may be evaluated over the flight-path angle domain where the solution is valid, with initial condition $\gamma = \gamma_0$, intermediate condition at V_C of $\gamma = \gamma_C$, and a final condition of $\gamma = \gamma_f = 0$:

$$\int_{\gamma_0}^{0} \frac{\rho V^2}{2\beta}(L/D)d\gamma \gg \int_{\gamma_0}^{\gamma_C} \left(\frac{V^2}{R} - g\right)\cos\gamma d\gamma + \int_{\gamma_C}^{0} \left(g - \frac{V^2}{R}\right)\cos\gamma d\gamma \tag{34}$$

Plugging in Eq. (12) and (7) into Eq. (34) results in expressions that are analytically integrable over the flight-path angle. The result of the integration is:

$$(L/D)\left[\left(\frac{\cos\gamma_0}{2H} - \frac{\rho_0(L/D)}{4\beta}\right)\left(V_f^2 - V_0^2\right) - \frac{2V_f^2 - V_0^2\left(2\cos\gamma_0 - (L/D)\sin\gamma_0\right)}{H\left(4 + (L/D)^2\right)}\right] \gg g\left(\sin\gamma_0 - 2\sin\gamma_C\right) + \frac{L/D}{R\left(4 + (L/D)^2\right)}\left[2V_f^2 - 2V_C^2\left(2\cos\gamma_C - \frac{L}{D}\sin\gamma_C\right) + V_0^2\left(2\cos\gamma_0 - \frac{L}{D}\sin\gamma_0\right)\right] \tag{35}$$

where the flight-path angle at the circular speed is:

$$\gamma_C = \gamma_0 - (L/D)\ln\left(V_C/V_0\right) \tag{36}$$

and V_f is the velocity at $\gamma = 0$:

$$V_f = V_0 \exp\left[\gamma_0/(L/D)\right] \tag{37}$$

Rearranging Eq (35) and writing the expression in terms of an assumption satisfaction factor f_L yields:

$$f_L = g\left(2\sin\gamma_C - \sin\gamma_0\right) + (L/D)\left(V_f^2 - V_0^2\right)\left[\frac{\cos\gamma_0}{2H} - \frac{\rho_0(L/D)}{4\beta}\right] - \frac{L/D}{\left(4 + (L/D)^2\right)}\times \left[2V_f^2\left(\frac{1}{R} + \frac{1}{H}\right) - \frac{2V_C^2}{R}\left(2\cos\gamma_C - \frac{L}{D}\sin\gamma_C\right) + V_0^2\left(\frac{1}{R} - \frac{1}{H}\right)\left(2\cos\gamma_0 - \frac{L}{D}\sin\gamma_0\right)\right] \gg 0 \tag{38}$$

In general, f_L should be much larger than zero for the steep lifting entry solution to be accurate for a particular vehicle configuration, initial condition, and planetary destination. If we further assume that ρ_0 is negligible relative to ρ, then the expression for f_L may be simplified to:

$$f_L = g\left(2\sin\gamma_C - \sin\gamma_0\right) + (L/D)\left(V_f^2 - V_0^2\right)\frac{\cos\gamma_0}{2H} - \frac{L/D}{\left(4 + (L/D)^2\right)}\times \left[2V_f^2\left(\frac{1}{R} + \frac{1}{H}\right) - \frac{2V_C^2}{R}\left(2\cos\gamma_C - \frac{L}{D}\sin\gamma_C\right) + V_0^2\left(\frac{1}{R} - \frac{1}{H}\right)\left(2\cos\gamma_0 - \frac{L}{D}\sin\gamma_0\right)\right] \gg 0 \tag{39}$$

Neglecting ρ_0 removes any dependence of f_L on ballistic coefficient.

In a similar manner, one can write the assumption that the drag term dominates the gravity term in Eq. (1a) as:

$$\frac{\rho V^2}{2\beta} \gg |g\sin\gamma| \tag{40}$$

This inequality may then be integrated over a trajectory, again using flight-path angle as the domain of integration. A negative sign is added to the right-hand side of Eq. (40) to ensure both sides are of the same sign, allowing the absolute value bars to be dropped:

$$\int_{\gamma_0}^{0} \frac{\rho V^2}{2\beta} d\gamma \gg -g\int_{\gamma_0}^{0} \sin\gamma d\gamma \tag{41}$$

Dropping the absolute value bars in this manner limits applicability of this relationship to trajectories with flight-path angles below zero. Unlike the previous derivation, both sides of this inequality remain positive for $\gamma \in [\gamma_0, 0]$. Applying the steep lifting entry solution to write V and ρ in terms of the flight-path angle and integrating yields:

$$\frac{V_0^2\left(2\cos\gamma_0 - (L/D)\sin\gamma_0\right) - 2V_f^2}{H\left(4 + (L/D)^2\right)} + \left(V_0^2 - V_f^2\right)\left(\frac{(L/D)\rho_0}{4\beta} - \frac{\cos\gamma_0}{2H}\right) \gg g\left(1 - \cos\gamma_0\right) \tag{42}$$

Rearranging and writing in terms of an assumption satisfaction factor f_D yields:

$$f_D = \frac{V_0^2\left(2\cos\gamma_0 - (L/D)\sin\gamma_0\right) - 2V_f^2}{H\left(4 + (L/D)^2\right)} + \left(V_0^2 - V_f^2\right)\left(\frac{(L/D)\rho_0}{4\beta} - \frac{\cos\gamma_0}{2H}\right) + g\left(\cos\gamma_0 - 1\right) \gg 0 \tag{43}$$

Neglecting ρ_0 relative to ρ results in a simpler expression:

$$f_D = \frac{V_0^2\left(2\cos\gamma_0 - (L/D)\sin\gamma_0\right) - 2V_f^2}{H\left(4 + (L/D)^2\right)} - \frac{\cos\gamma_0}{2H}\left(V_0^2 - V_f^2\right) + g\left(\cos\gamma_0 - 1\right) \gg 0 \tag{44}$$

As in Eq. (39), Eq. (44) shows that f_D is independent of β. The β-independence of f_L and f_D supports the assertion that ballistic coefficient does not directly impact the applicability of the steep lifting entry solution.

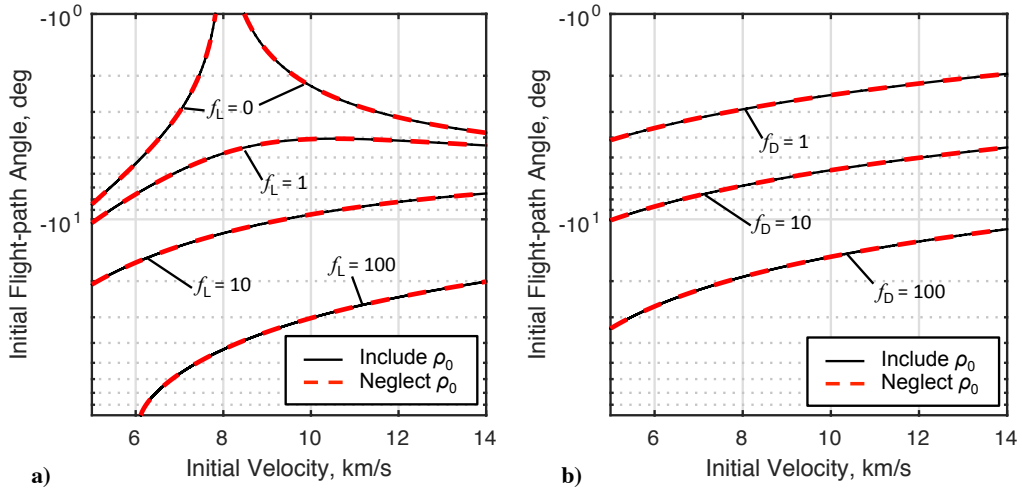

Figure 1. Contours of assumption satisfaction values over a range of initial conditions with and without the ρ_0 term for $\beta = 300$ kg/m^2, $L/D = 0.3$ at Earth: a) f_L and b) f_D.

Figure 1a shows contours of Eq. (38) and (39) over a range of initial conditions for a vehicle with a ballistic coefficient of 300 kg/m^2 and lift-to-drag ratio of 0.3 at Earth. Results indicate that neglecting ρ_0 is a good assumption–contours of Eq. (38) and (39) are indistinguishable. The assumption that the difference of the range-rate and gravity terms is small is a good assumption for $f_L \gg 0$, indicating that steeper, faster trajectories are more accurately approximated by the steep lifting entry solution. Figure 1b shows contours of Eq. (43) and (44) for the same scenario. Once again, neglecting ρ_0 appears to be an excellent assumption. Additionally, the assumption that drag is much larger than gravity during entry is more appropriate for steeper, faster trajectories, where $f_D \gg 0$. While specific values of f_L and f_D are meaningless, Fig. 1 shows clear trends for the applicability of the steep lifting entry solution.

The variation of contours of $f_L = 10$ and $f_D = 10$ with respect to lift-to-drag ratio os shown in Fig. 2a and b, respectively. In Fig. 2a, the region of applicability is the area beneath the contours for a given L/D. As L/D increases, the assumption becomes appropriate for a larger portion of the mission-design space. However, contours are mostly coincident for L/D greater than approximately 1. Figure 2b shows the opposite trend: lesser lift-to-drag ratios are associated with a larger region of applicability. This indicates that neglecting gravity's contribution to changes in velocity is a relatively poorer assumption for large L/D. Overall, Fig. 2 indicates that the assumptions inherent in the steep lifting entry solution are appropriate for a wide range of initial conditions and moderate-to-high values of L/D.

Contours of constant f_L and f_D may be overlaid to assess the size of the region in which both assumptions are satisfied, as shown in Fig. 3. The shaded region in Fig. 3 indicates the region for which both f_L and f_D are greater than or equal to 10 for an L/D of 2. This region is primarily bounded by the f_D contour. However, as L/D decreases, the boundary becomes dictated by f_L contours. The point at which this switch occurs at Earth is near an L/D of 1, as shown by the near-tangential intersection of the f_L and f_D contours in Fig. 3. For trajectories at Earth, lift-to-drag ratios below approximately one are more limited by the

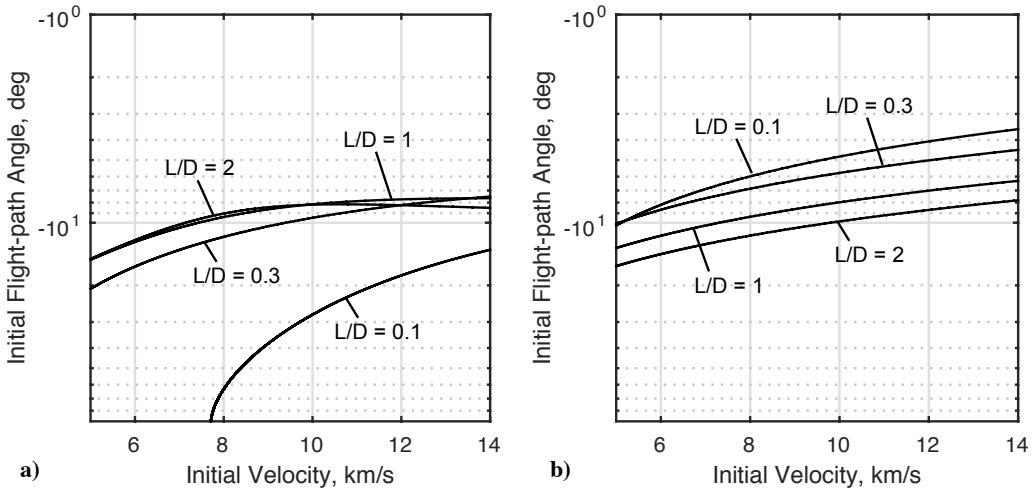

Figure 2. Contours of assumption satisfaction parameters over a range of initial conditions for several L/D at Earth: a) $f_L = 10$ and b) $f_D = 10$.

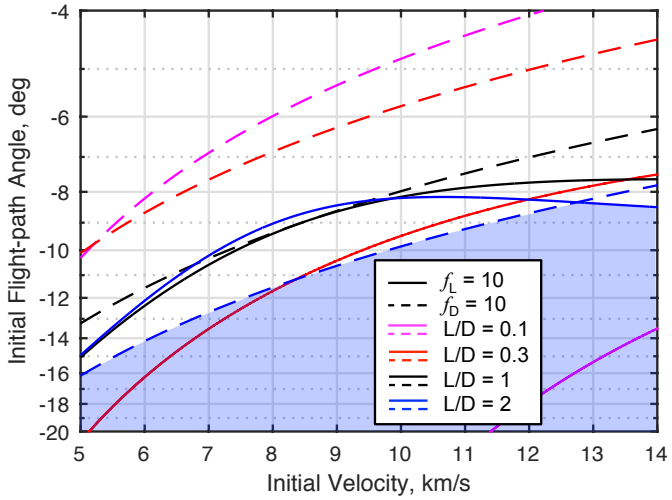

Figure 3. Assumption satisfaction values over a range of initial conditions for several L/D at Earth.

lift-equation assumption; lift-to-drag ratios above one are limited by some combination of the lift-equation and drag-equation assumptions.

The f_L and f_D expressions may be combined to identify regions in which both assumption satisfaction values are above a certain threshold. The combined assumption satisfaction value f_C is given by:

$$f_C = \min\left(f_L, f_D\right) \gg 0 \tag{45}$$

Figure 4 shows contours of $f_C = 1$ and $f_C = 10$ for several L/D. Higher values of f_C impose greater restrictions on the vehicle-mission design space, but also indicate that the assumptions are more appropriate. Figure 5 shows the same data on a larger, linear flight-path angle scale. This highlights that the steep-lifting entry solution is applicable across a wide range of initial conditions for moderate-to-large L/D.

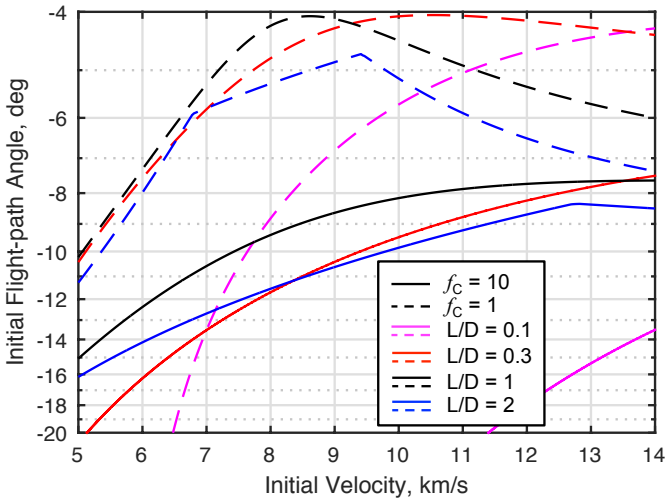

Figure 4. Contours of combined satisfaction value over a range of initial conditions for several L/D at Earth.

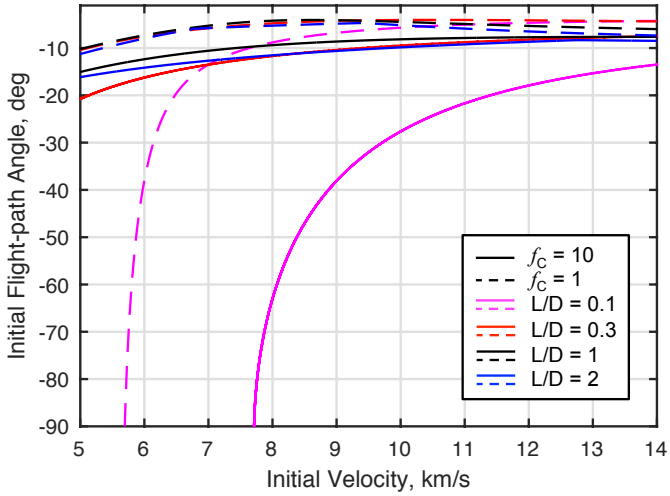

Figure 5. Contours of combined satisfaction value over a range of initial conditions for several L/D at Earth.

IV. Accuracy of Solution

Several example cases were selected to assess the accuracy of the steep lifting entry approximate solution relative to the planar equations of motion (see Table 2). The selected trajectories cover a range of planetary destinations, vehicle properties, and trajectory types. The strategic reentry vehicle (RV) is based on the

ballistic vehicle studied by King, but with an L/D of 0.5.[17] The L/D for the Apollo 10 vehicle is set to 60% of the maximum L/D and is consistent with Apollo entry guidance reference trajectory design.[18,19] The Venus aerocapture vehicle is selected from Craig and Lyne's parametric study.[20] The Viking trajectory is uniquely suited to the steep lifting entry solution, as it maintained a constant bank angle throughout its relatively steep entry at Mars.[21] The initial conditions for the trajectories have been moved forward such that the initial condition occurs after peak velocity is reached. This ensures monotonically decreasing velocity and increasing flight-path angle over the approximation region. Relevant planetary environment parameters are listed in Table 3.

Table 2. Example Trajectory Parameters

	Strategic RV[17]	Apollo 10[18]	Venus aerocapture[20]	Viking[21]
Planet	Earth	Earth	Venus	Mars
Initial velocity, km/s	7.2	11.085	13	4.72
Initial flight-path angle, deg	-30	-5.25	-6.8	-16.2
Initial altitude, km	30	90	230	90
Ballistic coefficient, kg/m^2	10,120	310	68	64
Lift-to-drag ratio	0.5	0.19	0.35	0.18

Table 3. Planetary Parameters

Planet	Venus	Earth	Mars
Radius, km	6,052	6,371	3,390
Surface g, m/s^2	8.87	9.80	3.71
Ref. density, kg/m^3	65	1.215	0.02
Ref. altitude, km	0	0	0
Scale height, km	15,900	7,500	11,100

A. Trajectory States

Figure 6 shows trajectories using the parameters in Table 2 computed using the steep lifting entry approximate solution (solid lines) and numerical integration of Eqs. (1) (dashed lines). Eqs. (1) are solved numerically using Matlab's intrinsic ode45 function with absolute and relative error tolerances of 10^{-9}.[22] The steep lifting entry solutions are generated using Eq. (6), (13), (15), and (29). The entry trajectories are approximated from the initial state near atmospheric interface to $\gamma = 0$. The aerocapture trajectory is approximated in two segments: atmospheric interface to $\gamma = 0$ and $\gamma = 0$ to atmospheric exit, where $\gamma = -\gamma_0$. While flight-path angle is a mathematically natural domain for the steep lifting entry solution, results are presented as a function of velocity for ease of interpretation. Figure 7 shows the absolute value of the percent error in the steep lifting entry solution relative to the planar equations of motion; spikes in the curves correspond to sign changes in the percent error.

Figure 6 indicates good agreement between the steep lifting entry solution and numerical integration for the strategic RV and Viking examples across all states. Percent error is below 5% for the strategic RV and below 10% for the Viking trajectory, with the exception of brief periods near the initial condition (in range, Fig. 7d) and end of the trajectories (in flight-path angle, Fig. 7b). Significant portions of the strategic RV trajectory exhibit error near 1%.

The Apollo 10 and Venus aerocapture examples are relatively shallow trajectories with relatively low L/D, resulting in poorer agreement with numerical integration. Unfortunately, low L/D and shallow entry flight-path angles are typical characteristics of current skip and aerocapture trajectories of interest. Altitude and range are reasonably well approximated for these cases, with error below approximately 12%. Flight-path angle and acceleration are not well approximated, with error exceeding 100% for significant portions of the trajectory. The error tends to increase quickly with decreasing velocity for all states for these examples.

While the percent error for the flight-path angle (Fig. 7b) is large, the magnitude of this error is only a few degrees (Fig. 6b). This remains a significant error, but the approximate solution does capture the general trends in the flight-path angle. Error tends to increase with decreasing velocity over most examples and states shown in Fig. 7.

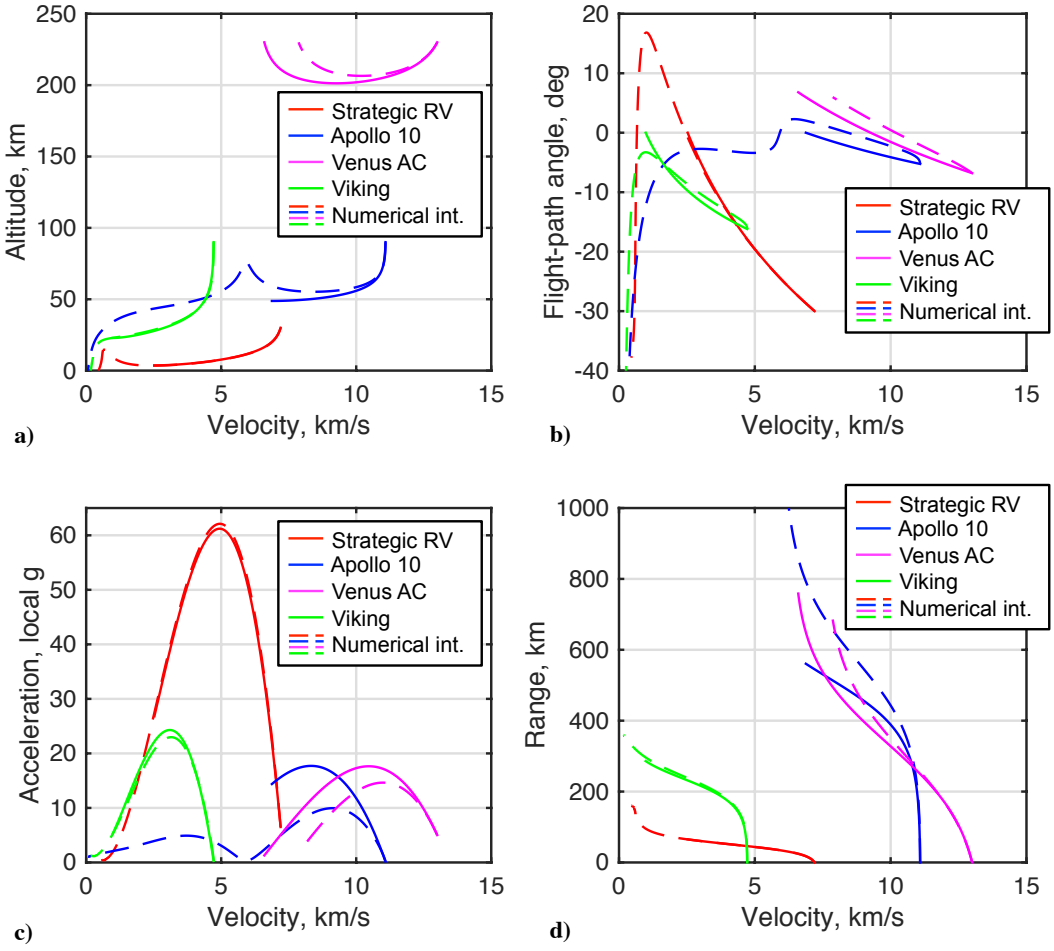

Figure 6. Comparison of steep lifting entry and numerical integration for several example trajectories over a) altitude, b) flight-path angle, c) sensed acceleration, and d) range versus velocity.

The work of Wang and Ting directly addresses Lees et al.'s solution's limited accuracy for trajectories with more shallow initial flight-path angles. Figure 8 shows density as a function of flight-path angle for the four example trajectories; Fig 9 shows the associated absolute percent error. The trajectories start at the triangle symbols; loops are caused by positive altitude rate in the trajectories. Wang and Ting's solution produces much better agreement with numerical integration than that of Lees et al. for the relatively shallow Apollo 10 and Venus aerocapture trajectories, reducing the percent error by an order of magnitude. For the steeper examples (strategic RV and Viking), neither version of the steep lifting entry shows clearly superior performance. In these cases, the solution of Lees et al. may be preferred for its relative simplicity. Overall, using the appropriate solution results in error below approximately 11% for all four examples. These expressions and their error are independent of any particular atmospheric density model, further enhancing their utility.

B. States at Peak Acceleration

Figure 10 shows the percent error (relative to numerical integration) in estimates of vehicle states at maximum acceleration for the four example trajectories. Figure 10a shows Wang and Ting's method is slightly more accurate in predicting peak acceleration across all four cases. The method of Lees et al. has lower error for

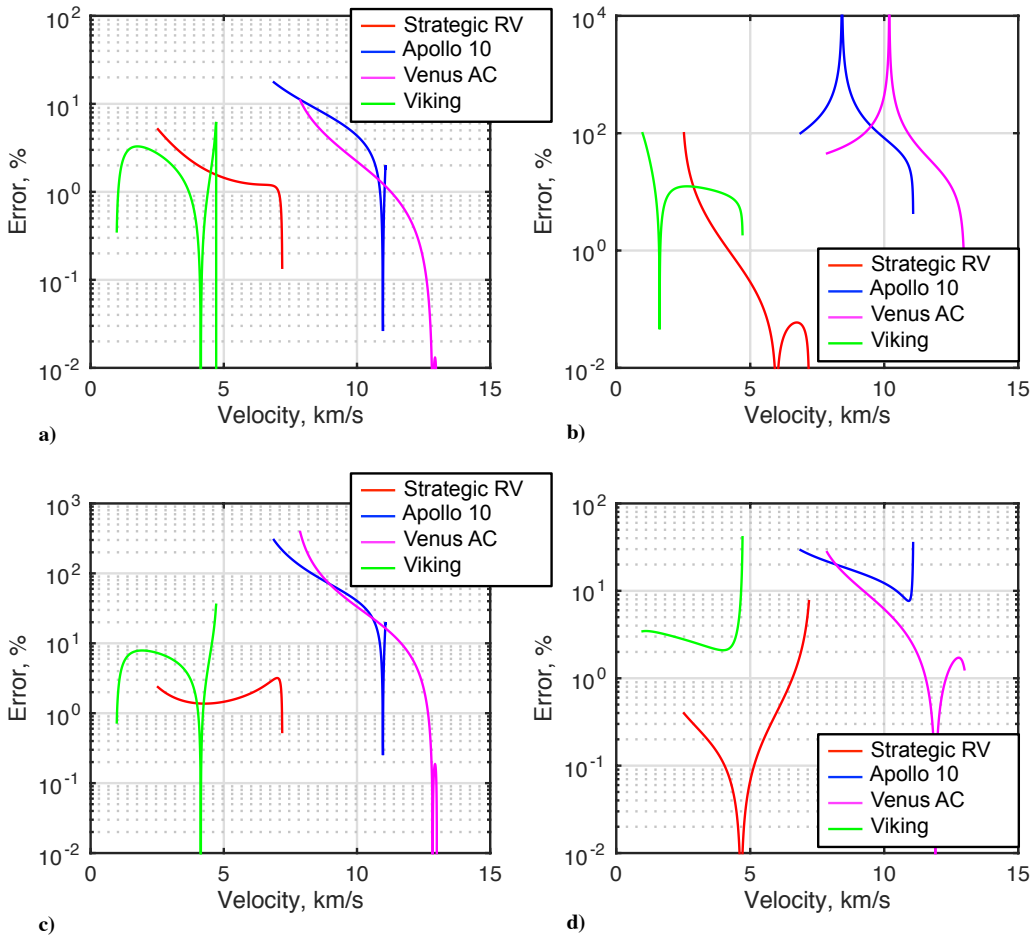

Figure 7. Absolute percent error in steep lifting entry approximate solution relative to planar equations of motion for a) altitude, b) flight-path angle, c) sensed acceleration, and d) range versus velocity.

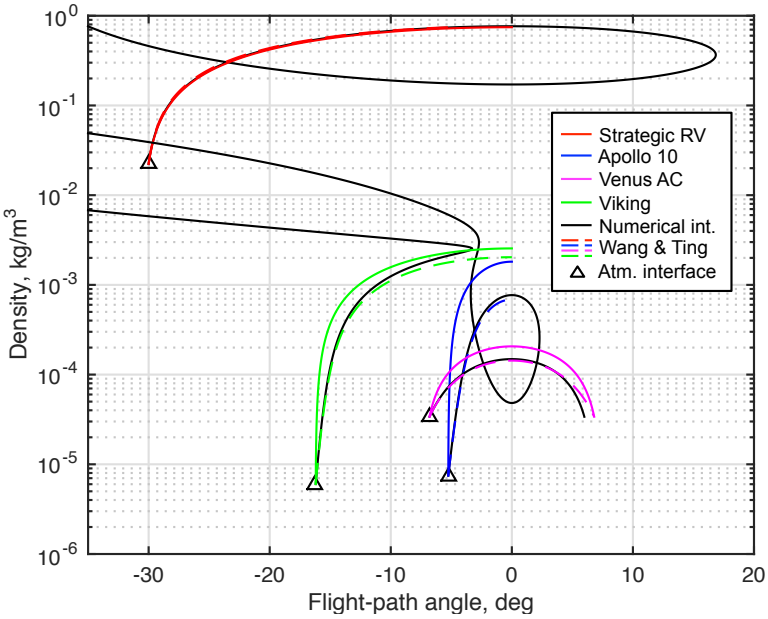

Figure 8. Comparison of Eggers et al., Wang and Ting, and numerical integration.

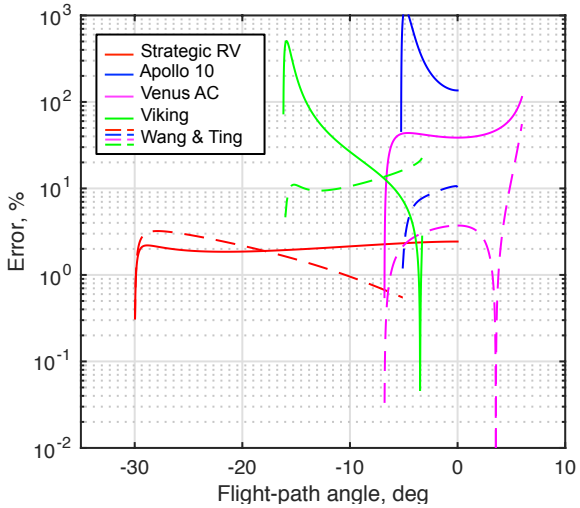

Figure 9. Comparison of density percent error relative to equations of motion for the solutions of Eggers et al. and Wang and Ting.

the velocity at peak acceleration (Fig. 10b). Wang and Ting's method shows significantly better accuracy in predicting the flight-path angle and density relative to the method of Lees et al. (see Fig. 10c and d) and is consistent with the accuracy demonstrated in Fig. 8.

Figure 11 shows contours of the percent error in estimation of the peak acceleration across a range of initial conditions for the example vehicles at their respective planets. Results are plotted against velocity normalized by the planet's circular velocity to facilitate comparison. As shown in Fig. 10, the solutions of Wang and Ting and Lees et al. exhibit similar accuracy for all four cases. For the strategic RV case, Fig. 11a shows nearly identical error behavior for the two methods. For the other three cases, Wang and Ting's method retains better accuracy for more shallow flight-path angles at greater entry velocities, although this difference is small.

Figure 12 shows the Wang and Ting solution error data from Fig. 11 co-plotted. Overall, trends across all four vehicles are similar. The steep lifting entry solution performs best for moderately steep initial flight-path angles at velocities above the circular speed. While the solution is theoretically applicable to aerocapture trajectories, the set of initial conditions corresponding to aerocapture trajectories exhibit poorer accuracy. Variation in ballistic coefficient appears to be the cause of the variation in percent error for velocities below circular velocity.

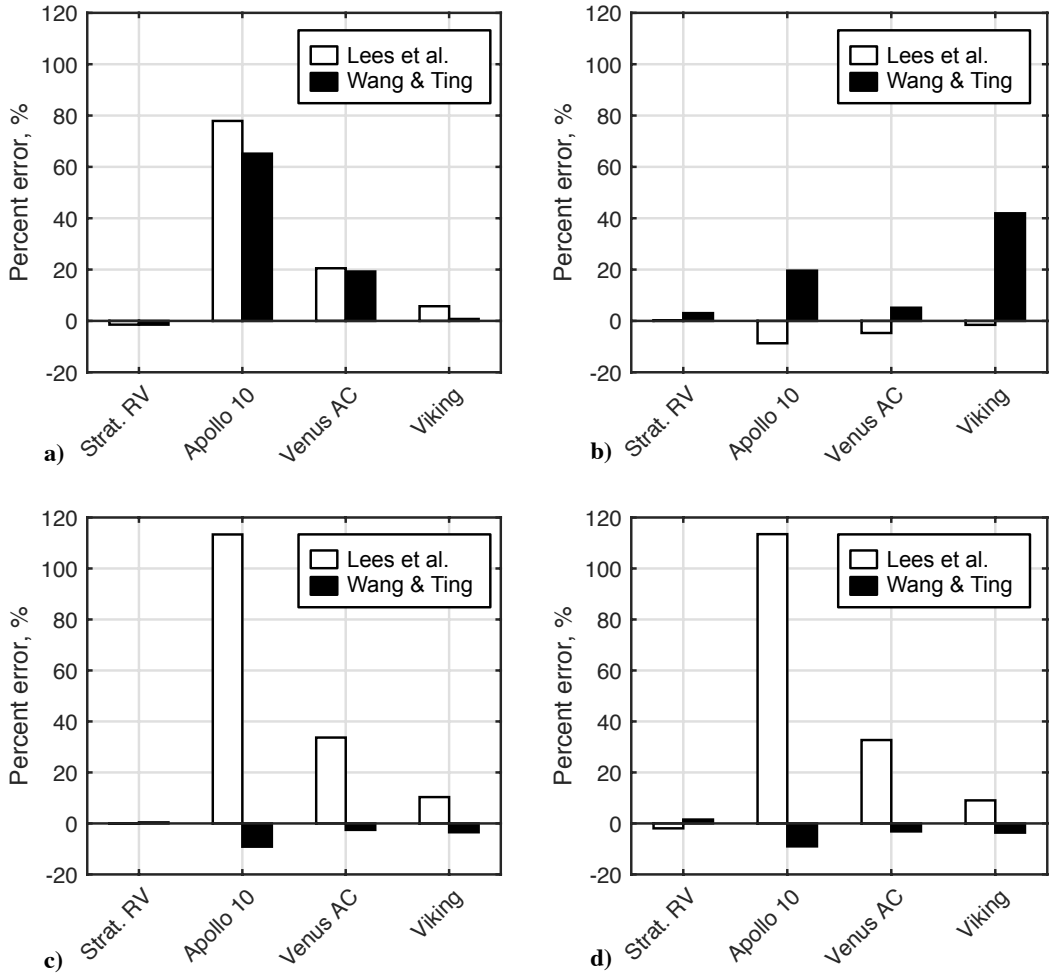

Figure 10. Percent error in vehicle states at peak acceleration relative to numerical integration for Lees et al. and Wang and Ting: a) peak acceleration magnitude, b) velocity, c) flight-path angle, and d) density.

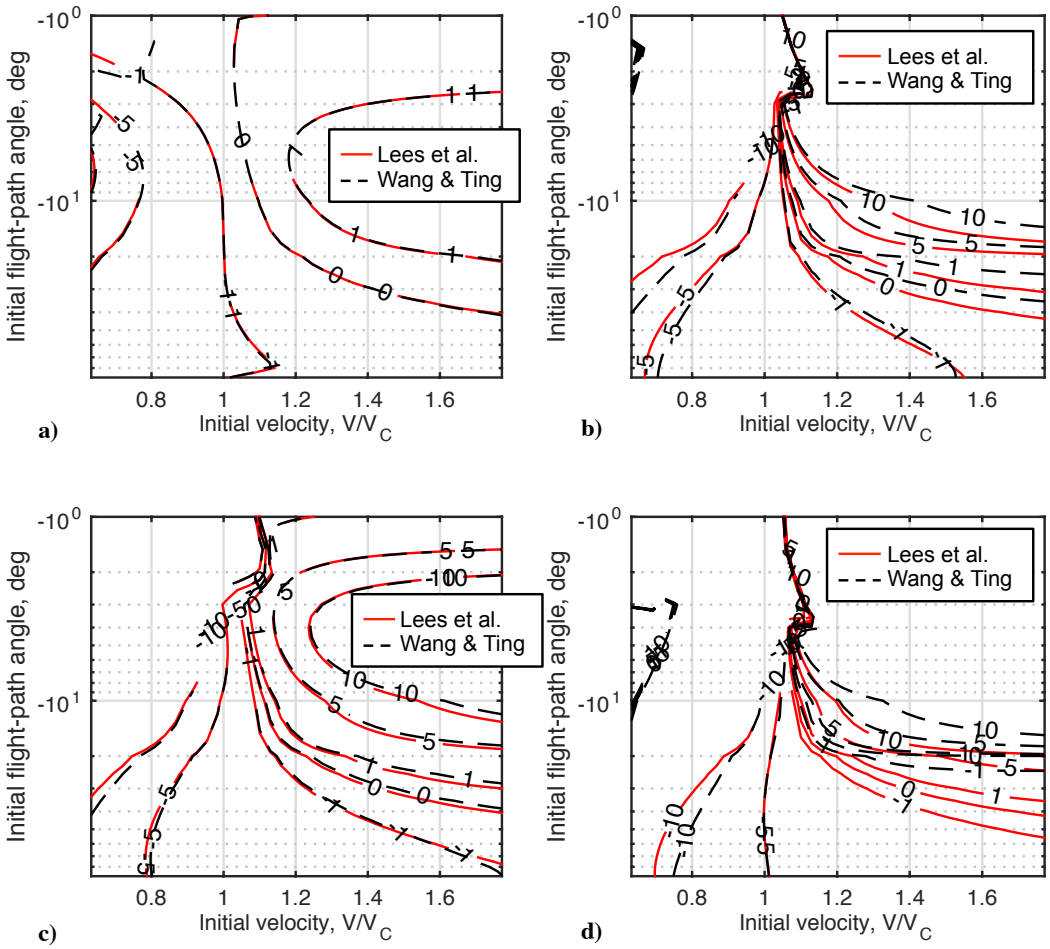

Figure 11. Percent error in peak acceleration estimates relative to numerical integration for Lees et al. and Wang and Ting for a) strategic RV, b) Apollo 10, c) Venus aerocapture, and d) Viking vehicles.

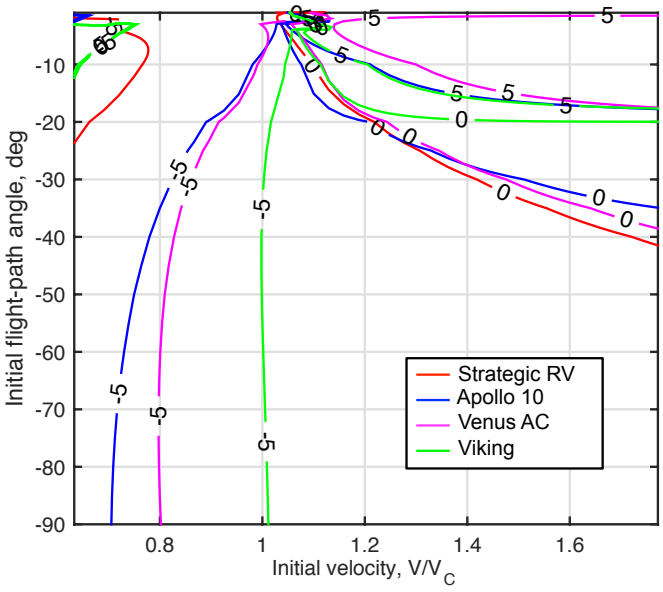

Figure 12. Percent error in peak acceleration estimates relative to numerical integration for several vehicles.

V. Conclusions

A complete treatment and derivation from first principles of the historical closed-form steep lifting entry trajectory solution was presented. Analytical assessment of the primary assumptions in the solution showed the solution is applicable across a wide range of initial trajectory states for vehicles with nonzero lift-to-drag ratios. The accuracy of the steep lifting entry solution relative to the planar equations of motion improves for steeper trajectories and larger lift-to-drag ratios. Prediction of density as a function of flight-path angle is particularly accurate. The steep lifting entry estimate of peak acceleration is shown to be accurate to within 10% for initial flight-path angles steeper than approximately -10 deg across a variety of vehicles and missions. Overall, the steep lifting entry solution provides a rapid first-order trajectory solution capability for lifting aeroassist vehicles with relatively steep initial flight-path angles that may be applicable for conceptual design and real time guidance and targeting applications.

Acknowledgement

This work was supported in part by a NASA Space Technology Research Fellowship.

References

[1]Ceruzzi, P. E., *Beyond the Limits: Flight Enters the Computer Age*, MIT Press, Cambridge, MA, 1989.

[2]Sänger, E. and Bredt, J. "A Rocket Drive for Long Range Bombers," Aug. 1944, Translated by M. Hamermesh, Technical Information Branch, Navy Dept., CGD-32.

[3]Loh, W. H. T., "A Second-Order Theory of Entry Mechanics Into a Planetary Atmosphere," *Journal of Aerospace Sciences*, Vol. 29(10), Oct. 1962, pp. 1210–1221.

[4]Citron, S. J. and Meir, T. C., "An Analytic Solution for Entry Into Planetary Atmospheres," *AIAA Journal*, Vol. 3(3), Mar. 1965, pp. 470–475.

[5]Eggers, A. J., Allen, H. J., and Neice, S. E., "A Comparative Analysis of the Performance of Long-Range Hypervelocity Vehicles," NACA R-1382, Washington, DC, 1958.

[6]Lees, L., Hartwig, F. W., and Cohen, C. B., "Use of Aerodynamic Lift During Entry Into the Earth's Atmosphere," *ARS Journal*, Vol. 29(9), Sep. 1959, pp. 633–641.

[7]Wang, K., and Ting, L., "An Approximate Analytic Solution of Re-Entry Trajectory With Aerodynamic Forces," *ARS Journal*, Vol. 30(6), Jun. 1960, pp. 565–566.

[8]Vinh, N. X., Johnson, W. R., and Longuski, J. M., "Mars Aerocapture Using Bank Modulation," AIAA 2000-4424, Aug. 2000.

[9]Miele, A., "Performance of Hypervelocity Vehicles," *Flight Mechanics*, Vol. 1, Addison-Wesley, Reading, MA, 1962, pp. 284–307.

[10]Vinh, N. X., Busemann, A., and Culp, R. D., "Analysis of First-Order Planetary Entry Solutions," *Hypersonic and Planetary Entry Flight Mechanics*, University of Michigan Press, Ann Arbor, MI, 1980, pp. 108-127.

[11]Regan, F. J. and Anandakrishnan, S. M.,"Re-Entry Vehicle Particle Mechanics, "*Dynamics of Atmospheric Re-Entry*, AIAA Education Series, American Institute of Aeronautics and Astronautics, Reston, VA, 1993, pp. 179–222.

[12]Eggers, A. J., Allen, H. J., and Neice, S. E., "A Comparative Analysis of the Performance of Long-Range Hypervelocity Vehicles," NACA RM-A54L10, Washington, DC, March 1955.

[13]Eggers, A. J., Allen, H. J., and Neice, S. E., "A Comparative Analysis of the Performance of Long-Range Hypervelocity Vehicles," NACA Technical Note 4046, Washington, DC, Oct. 1957.

[14]Lees, L., Hartwig, F. W., and Cohen, C. B., "The Use of Aerodynamic Lift During Entry Into the Earth's Atmosphere," Space Technology Laboratories, GM-TR-0165-00519, Los Angeles, CA, Nov. 20, 1958.

[15]Wang, K., and Ting, L., "Approximate Solutions for Reentry Trajectories With Aerodynamic Forces," Polytechnic Institute of Brooklyn Aeronautical Laboratory Report No. 647, Brooklyn, NY, May 1961.

[16]Allen, H. J. and Eggers, A. J., "A Study of the Motion and Aerodynamic Heating of Ballistic Missiles Entering the Earth's Atmosphere at High Supersonic Speeds," NACA R-1381, Washington, DC, 1958.

[17]King, H. H., "Ballistic Missile Re-Entry Dispersion," *Journal of Spacecraft and Rockets*, Vol. 17(3), May 1980, pp. 240–247.

[18]Graves, C. A. and Harpold, J. C., "Apollo Experience Report–Mission Planning for Apollo Entry," NASA TN D-6725, Washington, DC, Mar. 1972.

[19]Morth, R., "Reentry Guidance for Apollo," MIT Instrumentation Laboratory R-532, Cambridge, MA, Jan. 1966.

[20]Craig, S. and Lyne, J. E., "Parametric Study of Aerocapture for Missions to Venus," *Journal of Spacecraft and Rockets*, Vol. 42(2), Nov. 2005, pp. 1035–1038.

[21]Braun, R. D. and Manning, R. M., "Mars Exploration Entry, Descent, and Landing Challenges," *Journal of Spacecraft and Rockets*, Vol. 44(2), Mar. 2007, pp. 310–323.

[22]Matlab, Ver. 8.4.0.150421 (R2014b), The Mathworks, Inc., Natick, MA, 2014.